

Role of local climate zones and urban ventilation in canopy urban heat island–heatwave interaction in Nanjing megacity, China

Weishou Tian^a, Yuanjian Yang^a, Linlin Wang^{a,b,*}, Lian Zong^a, Yanhao Zhang^a, Duanyang Liu^c

^a Collaborative Innovation Centre on Forecast and Evaluation of Meteorological Disasters, School of Atmospheric Physics, Nanjing University of Information Science & Technology, Nanjing 210044, China

^b State Key Laboratory of Atmospheric Boundary Layer Physics and Atmospheric Chemistry (LAPC), Institute of Atmospheric Physics, Chinese Academy of Sciences, Beijing 100029, China

^c Key Laboratory of Transportation Meteorology of China Meteorological Administration, Nanjing Joint Institute For Atmospheric Sciences, Nanjing 210041, China

ARTICLE INFO

Keywords:
Canopy urban heat island
Heat wave
Local climate zone
Wind speed
Urban heat advection
Nanjing

ABSTRACT

Different local climate zones (LCZs) and wind speeds (WSs) increase the uncertainties related to canopy urban heat island (CUHI), heat waves (HWs), and their interactions. Taking the megacity of Nanjing in China as an example, this paper quantifies and elucidates the spatiotemporal variations of the CUHI intensity (CUHII) and its association with HWs, as well as their potential drivers. Results show a significant diurnal variation in CUHII, showing a valley at daytime and a peak at nighttime. The CUHII is significantly stronger in the HW periods than in the non-heatwave (NHWs) periods, especially at daytime, which is a positive feedback to HW intensity. The interannual variability of CUHII was mainly dominated by anthropogenic heat emissions and air pollutions. While the spatial patterns of mean CUHII and HWs were shaped by LCZs and urban ventilation. Over LCZs with high densities of buildings in the city center, the CUHII is higher and HW events are more frequent under medium-low WS than high WS. In contrast, over LCZs with an open distribution of buildings on the urban outskirts, under high WS condition, CUHII becomes higher and HW events become more frequent relative to low WS, due to the high wind-driven heat advection.

1. Introduction

More than half of the population lives in urban areas all over the world, and this proportion is expected to increase to about 70% by 2050, with the continued emergence of urban agglomerations and rural-to-urban migration (United Nations, 2019). The urban energy balance is altered due to rapid urbanization; more heat is absorbed/generated/stored, resulting in high temperatures in cities compared to the surrounding rural/suburban areas, and leading to increasingly significant urban heat island (UHI) effects (Arnfield, 2003; Oke et al., 2017; Santamouris, 2015). The temperature increase caused by UHIs has many negative impacts on human society, which are further amplified by heat waves (HWs) (Poumadère et al., 2005; He et al., 2021; Li and Bou-Zeid, 2013). In recent years,

* Corresponding author at: Collaborative Innovation Centre on Forecast and Evaluation of Meteorological Disasters, School of Atmospheric Physics, Nanjing University of Information Science & Technology, Nanjing 210044, China.

E-mail address: linlinwang@mail.iap.ac.cn (L. Wang).

many cities have faced the threat of overheating from both UHIs and HWs (Kumar and Mishra, 2019; Chew et al., 2021; Jiang et al., 2019). Exposure to extreme-heat events often results in uncontrolled thermal regulation of the inhabitants, leading to physiological heat stress and increasing heat-related mortality and morbidity (Basagaña et al., 2011; Cedeño Laurent et al., 2018; Thompson et al., 2018; Vicedo-Cabrera et al., 2021). In addition, overheating also causes a devastating impact on energy consumption, economies, and the environment (Francisco et al., 2017; Santamouris, 2020). Therefore, the study of UHIs and HWs has received increasing attention in recent years in various countries around the world (Oke and Runnalls, 2000; Tan et al., 2010; Imran et al., 2019).

Global warming and the impacts of canopy UHIs (CUHIs) potentially enlarge the spatiotemporal coverage of high temperatures in cities, and thus there is a tendency for extreme-heat events to spread with more intense, frequent, and prolonged HWs over urban areas (Habeeb et al., 2015; Shafei Shiva et al., 2019; Perkins et al., 2012). Amplification of the canopy UHI intensity (CUHII) during HWs has been recorded in many cities around the world (Gao et al., 2019; Pyrgou et al., 2020), especially at nighttime. For example, compared to non-heat-waves (NHWs), a significant increase in CUHII during HWs was found at nighttime in Beijing (Li et al., 2015) and Karachi (Rizvi et al., 2019). Meanwhile, increased CUHII was found in the daytime during HWs in Sydney (Khan et al., 2020), Shanghai (Ao et al., 2019), and Athens (Founda and Santamouris, 2017). Generally, the synergy of CUHI–HW interaction is attributed to differential responses of urban–rural surface energy balances to overheating (He et al., 2019), which is usually also closely related to underlying surface features (Guo et al., 2020; Santamouris, 2014), meteorological conditions (Huang et al., 2020), and ecological conditions (Yang et al., 2019; Yun et al., 2020). Therefore, it can be deduced that CUHIs, HWs, and their interactions are highly dependent on local climate zones (LCZs).

As an objective and systematic classification of field sites for CUHI studies, the LCZ system was proposed by Stewart and Oke (2012). In cities, LCZs can reveal the differences in the internal three-dimensional urban structure and surface materials, which seriously affect the accurate assessment of climatic and environmental effects and hinder regional comparative studies of CUHIs on a global scale (Stewart, 2011; Kaloustian and Bechtel, 2016; Xz et al., 2020). The LCZ classification, which has been extensively developed by the World Urban Database and Access Portal Tool (WUDAPT) project, is used as a standardized and common framework for collecting data on global urban form (Ma et al., 2020). In China, the concept of LCZs has standardized the calculation of CUHIs and the link between urban morphology, surface properties, and CUHIs has been initially established (Hu et al., 2019), which is favorable for exploring the synergistic interactions of CUHI–HWs and LCZs.

The factors regulating CUHIs and HWs are complex and variable on spatial and temporal scales, but can generally be divided into natural factors [local topography, ecology, and meteorological factors such as wind speed (WS), wind direction, cloud cover, relative humidity, etc.] (Wang et al., 2020a; Manoli et al., 2019) and anthropogenic factors (e.g., anthropogenic heat emissions, aerosol emissions, urbanization, etc.) (Li and Zhao, 2012; Guo et al., 2021). Considering that HWs are usually generated owing to the existence of large-scale, stagnant high-pressure systems, resulting in prolonged temperature anomalies across the region (Black et al., 2004; Meehl and Tebaldi, 2004), there is an association with local WS conditions. The mechanisms of the mitigative effect of WS are well-known, being mainly associated with wind influencing atmospheric transport and mixing in the urban canopy layer. Wind-induced vertical transport and turbulent mixing disrupt the heat balance of the urban heat, thereby facilitating the mixing of urban and rural air. This results in the inflow of cold rural air into urban areas or the escape of warm urban air into rural areas, both of which can significantly reduce the CUHI (He, 2018; Ngarambe et al., 2021). However, the mechanism of wind mitigation may be uncertain when considering urban heat advection (UHA) caused by various wind directions. UHA can be considered as the heat resulting from the windborne transport of energy within the urban environment (Oke et al., 2017). The following surface energy balance equation extends from the infinitesimal interface layer below the surface to a certain volume of outdoor space at the top of the building:

$$R_n + AF + HA = H + LE + G \quad (1)$$

where R_n is the net radiation, AF is the anthropogenic heat in the volume, HA is the net UHA, and the total output is divided into sensible heat flux H , latent heat flux LE , and stored heat flux G (Wang et al., 2020b). Thus, the UHA caused by wind according to the energy balance equation may be a key factor in regulating the urban heat.

Nanjing, as an East Asian, subtropical, inland, developed city and one of the four famous “furnaces”, is a typical study area for analyzing high temperatures and their factors of influence. CUHIs and HWs in Nanjing megacity have been studied by many scientists (Huang et al., 2008; Tu et al., 2016; Chen et al., 2015; Wu et al., 2017; Chen et al., 2022). Since the reform and opening up of China in 1978, Nanjing has experienced rapid urbanization and a surge in population along with economic development, and the mean CUHII in the built-up area of Nanjing has already been observed to be around 0.68 °C, with significant diurnal variation characteristics (Chen et al., 2022). The CUHII in Nanjing has a maximum peak from sunset to about 2 h after sunrise, and a minimum peak or even negative value from 2 h after sunrise to sunset (Yang et al., 2020). Furthermore, the duration and average intensity of high temperatures in Nanjing have been found to be increasing year by year, and HWs are mainly concentrated in August (Liu et al., 2015). It is preliminarily understood that Yang et al. (2018) used the LCZ classification for the first time in the study of the thermal environment of Nanjing. However, there are still three issues with respect to the summertime CUHI in Nanjing that have yet to be fully understood—namely, the synergy of CUHI–HW interaction in Nanjing; the interclass differences in CUHIs and HWs in LCZs; and the effects of meteorological factors (e.g., WS) on CUHIs and HWs and their interactions.

Taking Nanjing megacity as an example, therefore, this paper, combined with the LCZ classification and WS, shows the synergy of CUHI–HW interaction in Nanjing based on automatic weather station observations during the summers (June–September) of 2015–2020. Our findings have important implications and offer scientific guidance for improving the urban thermal environment, adjusting the energy structure, and adapting to the public health risk in high-density megacities. Following this introduction, Section 2 describes the various observational data and methods used in the study. Section 3 examines the diurnal and interannual variations of

the CUHI and their associations with different LCZs and WS. The possible drivers are then discussed in [Section 4](#), followed by concluding remarks in [Section 5](#).

2. Data and methods

2.1. Study area and observational data

Nanjing (32°49'N, 118°48'E) is located in the Yangtze River Delta region, at the lower reaches of the Yangtze River, and is one of the more modern and economically developed megacities in China. According to government data, in 2020, the urban area of Nanjing was about 868 km², and the rate of green coverage of the built-up area reached 45.2%, showing an increasing trend year on year. The urban population exceeded 8 million, and the rate of urbanization reached 86.8%, with the same year-on-year increasing trend. Nanjing is located in the subtropical monsoon climate zone, with four distinct seasons, abundant precipitation, and an average daily temperature throughout the year of 28.1 °C (July) to 2.7 °C (January). The topography of Nanjing includes hills, plains, rivers, and lakes. The main urban area is located on the south side of the Yangtze River, which is relatively flat, within 30 m above sea level, and mostly densely built-up. The Yangtze River flows through the western and northern sides of Nanjing's urban area; the main bodies of water in the city include Xuanwu Lake, Qinhui River, among others; and the city is surrounded by mainly flat agricultural and industrial land ([Fig. 1](#)).

In addition, it is also worth noting that most residential buildings and small office buildings in Nanjing use air conditioning for cooling in summer, and large public buildings usually use central air conditioning systems ([Yang et al., 2020](#)).

As one of the fastest growing metropolises in inland China in recent decades, the rapid urbanization of Nanjing has led to a significant growth of infrastructure such as buildings and roads, and the urban area has become an area of dense construction and large

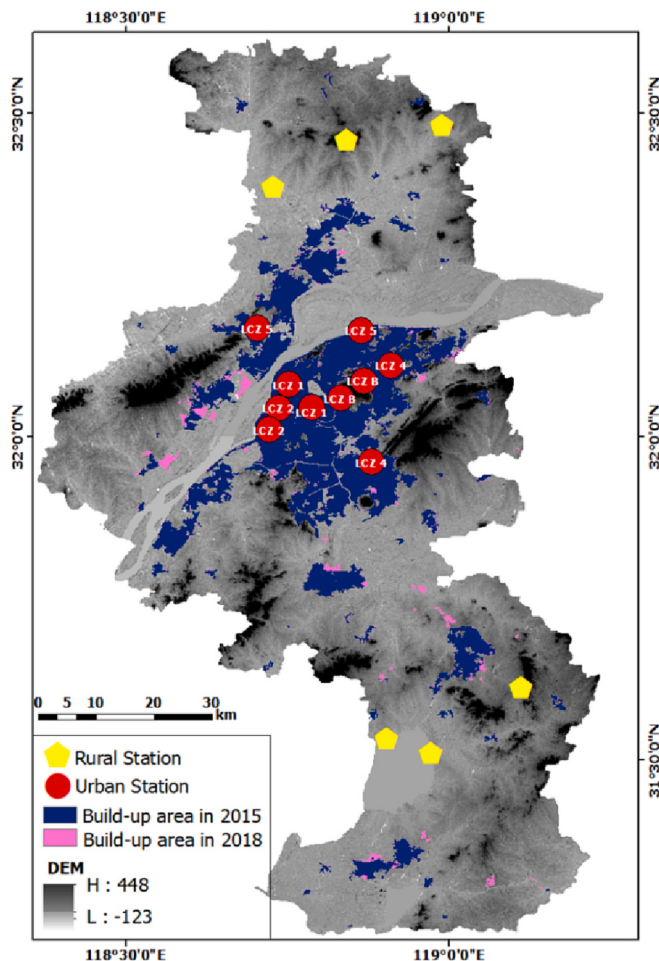


Fig. 1. The spatial distribution of automatic weather stations based on the built-up area of Nanjing in 2015 and 2018, with red circles representing urban stations and yellow pentagons representing rural stations. (For interpretation of the references to colour in this figure legend, the reader is referred to the web version of this article.)

quantities of anthropogenic heat emissions (Figs. 1 and 2). Ten urban automatic weather stations and six rural stations were selected, and hourly weather data (including surface air temperature and surface WS and wind direction) during summer 2015–2020 (June–August) were downloaded from <http://data.cma.cn/en>. The observed data of PM10 in summer (June–August) of 2015–2020 were retrieved from Nanjing Ecological Environment Monitoring Center. 2015–2020 population data of Nanjing were retrieved from Nanjing Statistical Yearbook. The anthropogenic heat flux (AHF) in Nanjing was estimated with satellite data using the RAHF (Refined Anthropogenic Heat Flux) model, including anthropogenic heat sources of industrial activities, heating and cooling of buildings, human metabolism, and traffic emissions. Similarly, the mean AHF, NDVI, and the built-up area ratio in a buffer zone with a 2-km radius around each station were calculated (Table 1).

Stations were located in different areas with unique physical characteristics. Ten urban stations and six rural stations were initially selected by viewing satellite images and field visits. The principles for selecting suitable urban stations were:

- A) The area within a radius of 200–500 m should be as reasonable and unified as possible in terms of surface structure, land cover, building materials, and land functions.
- B) The selected LCZ categories should be diverse enough and representative enough to improve the comprehensiveness of the study.
- C) The mean AHF, NDVI, and built-up area ratio within the buffer are important references for selecting stations (Table 1).

The method described in Xu et al. (2013) was used for quality control and homogenization of the daily meteorological data.

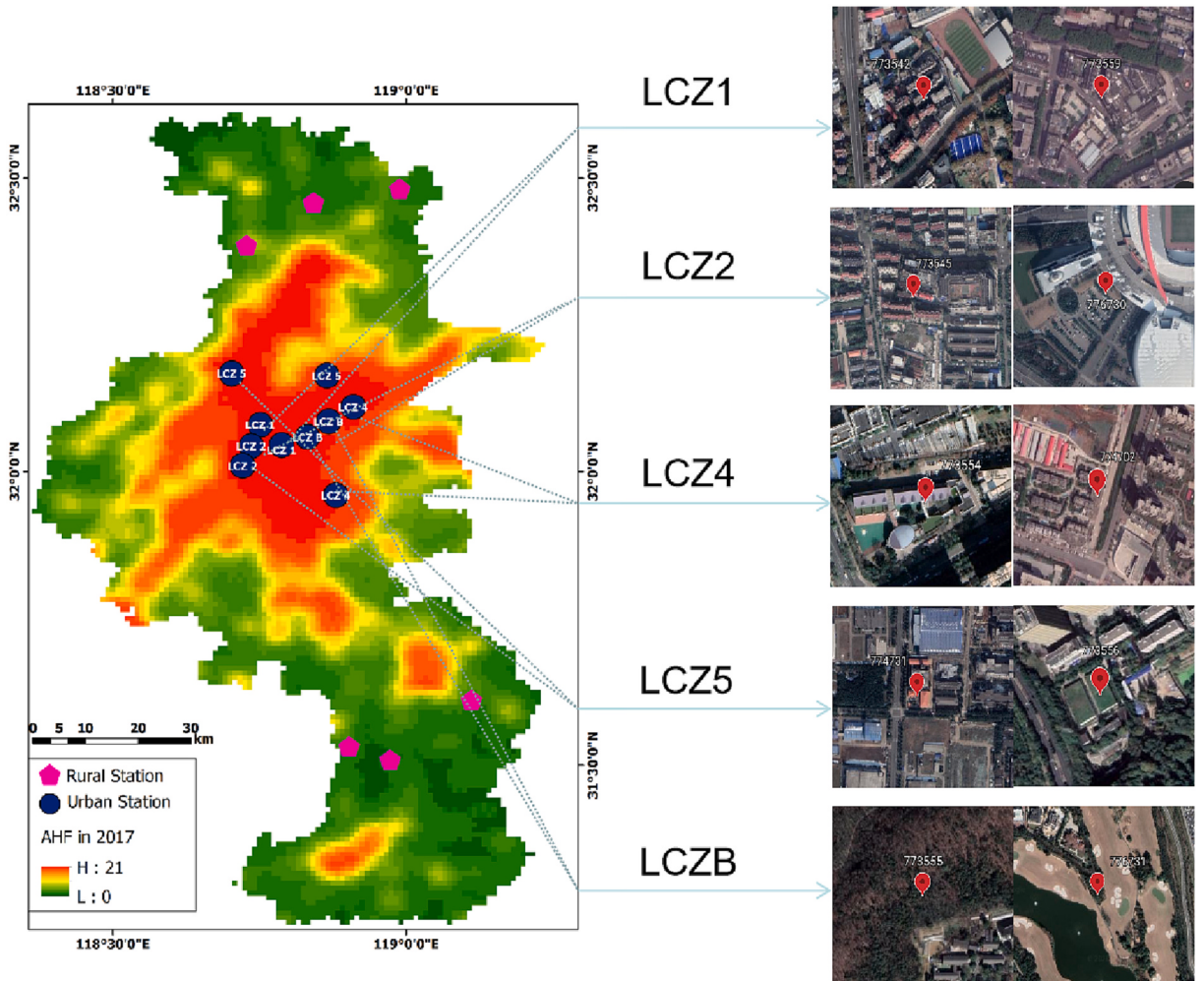


Fig. 2. The spatial distribution of automatic weather stations based on anthropogenic heat emissions of Nanjing in 2017 and the specific urban canopy structure (images from Google Earth).

Table 1

Specific locations of selected automatic weather stations and the mean values of AHF, NDVI, and built-up area ratio within 2 km.

Num	Sta	Lon	Lat	LCZ	AHF (w/m^2)	NDVI	Build-up area(%)	Key variables
St-1	773,542	118.75	32.08	LCZ 1	21	0.3728	99.98	Residential areas; Compact high-rise
St-2	773,559	118.78	32.04	LCZ 1	21	0.3312	99.98	Commercial streets; Compact high-rise
St-3	773,545	118.73	32.04	LCZ 2	21	0.3582	96.84	Residential areas; Compact mid-rise
St-4	776,730	118.72	32.01	LCZ 2	21	0.4051	99.97	Gymnasium; Compact mid-rise
St-5	773,554	118.91	32.11	LCZ 4	21	0.4774	83.51	Residential areas; Open high-rise
St-6	774,702	118.88	31.96	LCZ 4	20.47	0.3944	86.15	Residential areas; Open high-rise with paved
St-7	774,731	118.70	32.16	LCZ 5	21	0.3607	80.07	Industrial areas; Open mid-rise
St-8	773,556	118.86	32.16	LCZ 5	20.41	0.3444	61.41	Residential areas; Open mid-rise with paved
St-9	773,555	118.83	32.05	LCZ B	20.94	0.7385	11.54	City park; Scattered trees
St-10	776,731	118.86	32.08	LCZ B	20.59	0.6429	56.13	City park; Scattered trees

2.2. Research methods

In our study, the CUHII was quantified by using the CUHII, which is defined as the difference between the temperature of each urban station and the mean temperature of the six rural stations. Although this urban–rural method provides a simple, systematic way to quantify the CUHII, the premise is that suitable rural reference stations must be selected to avoid inaccurate CUHIs. Usually, rural stations should be located in relatively flat terrain, and there should be almost no difference in elevation between urban and rural stations to reduce the error caused by elevation. In addition, the latitude of the selected stations should be considered. Three rural stations are located north of the urban area and three are located south to offset the error caused by latitude. To reduce the above potential errors, we employed mean temperature of the six rural stations as reference values to calculate the CUHII. The surrounding natural environment, the absence of impermeable surfaces, and the absence of dense buildings common in urbanized areas were also considered.

In addition, different methods are used to study HWs in different regions of the world, and there is currently no uniform HW standard globally. An HW event is usually defined as the daily maximum temperature reaching or exceeding a certain threshold for several consecutive days (Ngarambe et al., 2020). The HW event in this paper is defined as the daily maximum temperature exceeding 35 °C for three consecutive days or more, as described in Jingxin et al. (2020).

To research the potential influence of urban spatial structures and land-cover types on the CUHI–HW interaction, the LCZ

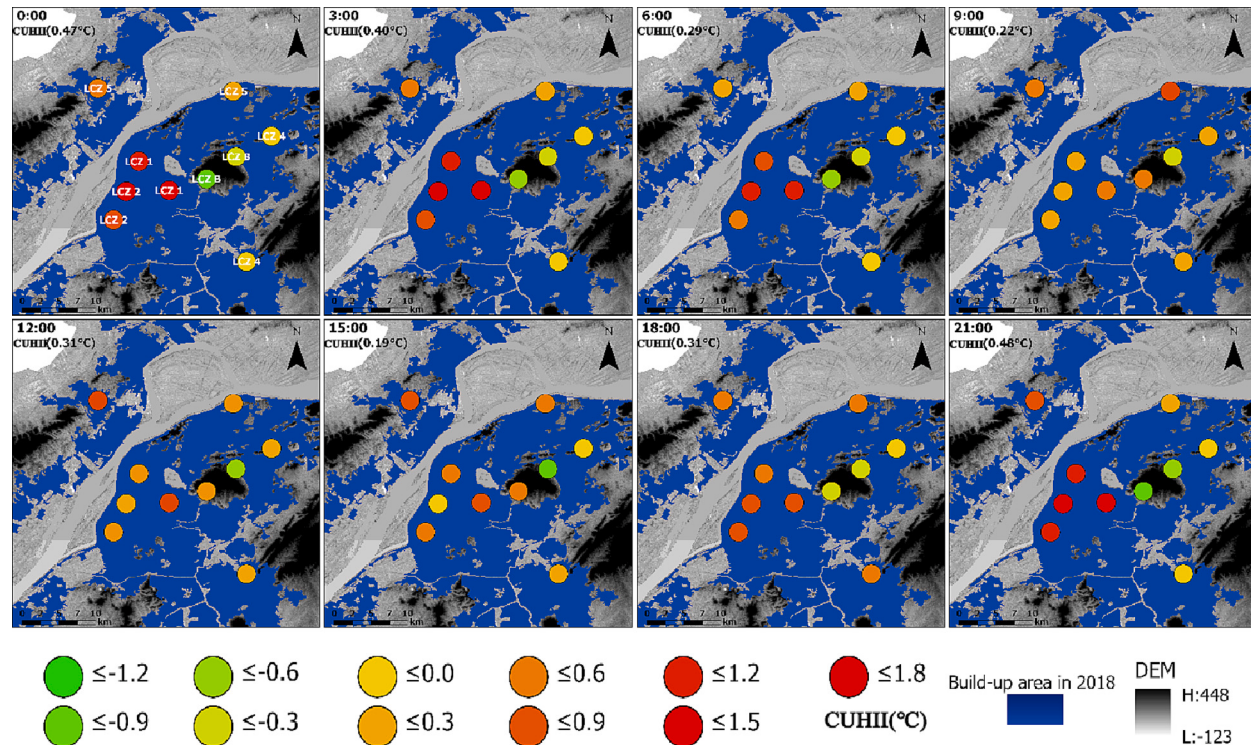


Fig. 3. Diurnal variation characteristics of the CUHII in Nanjing. The mean CUHII of 10 stations is given in the top-left corner. The blue shading areas indicates the density of the built-up areas of Nanjing, and the gray-black shadings indicate altitudes. (For interpretation of the references to colour in this figure legend, the reader is referred to the web version of this article.)

categories of the selected stations were obtained from the LCZ dataset produced by the Institute of Urban Meteorology, China Meteorological Administration, Nanjing. According to the workflow provided by WUDAPT, fine subsurface data were derived in SAGA GIS by performing Random Forest classification of the Landsat8 satellite data. Based on the surface features of urban climate proposed by previous studies (Stewart and Oke, 2012; Stewart et al., 2014; Zong et al., 2021), the LCZ dataset consisted of 17 types with significant differences. The five most common LCZ categories in Nanjing were selected (i.e., LCZ1, LCZ2, LCZ4, LCZ5, and LCZB), and two urban stations for each LCZ category (Fig. 1 and Table 1), which are denoted by St-1 to St-10 in the following analysis. In addition, the surface structure of the urban LCZB type is similar to that of the rural area, but there are huge differences between them. The urban LCZB may be in a forest park or wetland, but it is still in the center of the city alongside many urban buildings and anthropogenic heat emissions. Whereas, the rural sites are far from urban built-up areas and are less affected by human activities. More specifically, the selection of urban LCZB types provides strong evidence that urban green spaces and water bodies are effective in alleviating UHIS (Doick et al., 2014).

In our study, the potential effects of WS on the CUHII and HW, along with their interactions, were investigated by classifying the WS at the national station (58238) into three categories using a k-means clustering algorithm: low WS (0–2.2 m/s), medium WS (2.2–3.5 m/s), and high WS (> 3.5 m/s). Finally, we used an analysis of variance (ANOVA) test to assess differences in UHII across WSs and LCZ categories, with statistical significance at the 0.001 confidence level. In addition, in order to further explore the potential impact of urban ventilation on UHA, this paper introduces the WS ratio (WSR) index [WSR = WS/WS_r (Liu et al., 2022b; Yang et al., 2013)]. Where WS represents WS (m/s) of urban station, WS_r is the average WS of rural stations, and this index effectively reflects the urban ventilation capacity. At the same time, the stability of surface wind is used to test UHA, and the urban surface transport index (USTI) is introduced to link the stability of wind with its transport capacity to urban heat. The calculation method of USTI is as follows:

$$USTI = \frac{\sqrt{(\sum_{i=1}^n u_i)^2 + (\sum_{i=1}^n v_i)^2}}{\sum_{i=1}^n \sqrt{u_i^2 + v_i^2}} \quad (2)$$

where u , v , and n denote zonal and meridional wind speed, and number of urban stations, respectively (Berkovic, 2016).

3. Results

3.1. Diurnal variation

Based on the hourly mean CUHII at 10 urban stations in Nanjing during summertime [0000, 0300, 0600, 0900, 1200, 1500, 1800 LST (local standard time)] in the period 2015–2020, Fig. 3 shows the diurnal variation characteristics of the CUHII, indicating that the CUHII is strong during the nighttime, while weak during the daytime. In addition, a secondary peak occurs at 1200 LST, and the same conclusion is drawn by calculation. The peak mean CUHII is around 0.5 °C at 2000–2100 LST, and the lowest mean CUHII is around 0.15 °C at 1500–1600 LST. Additionally, the station near the Yangtze River (St-1) in the two LCZ1 type stations has a weaker CUHII (mean CUHII of 0.7 °C for St-1 and 1.12 °C for St-2 in LCZ1) compared to the other station. Note that the two LCZB stations are in

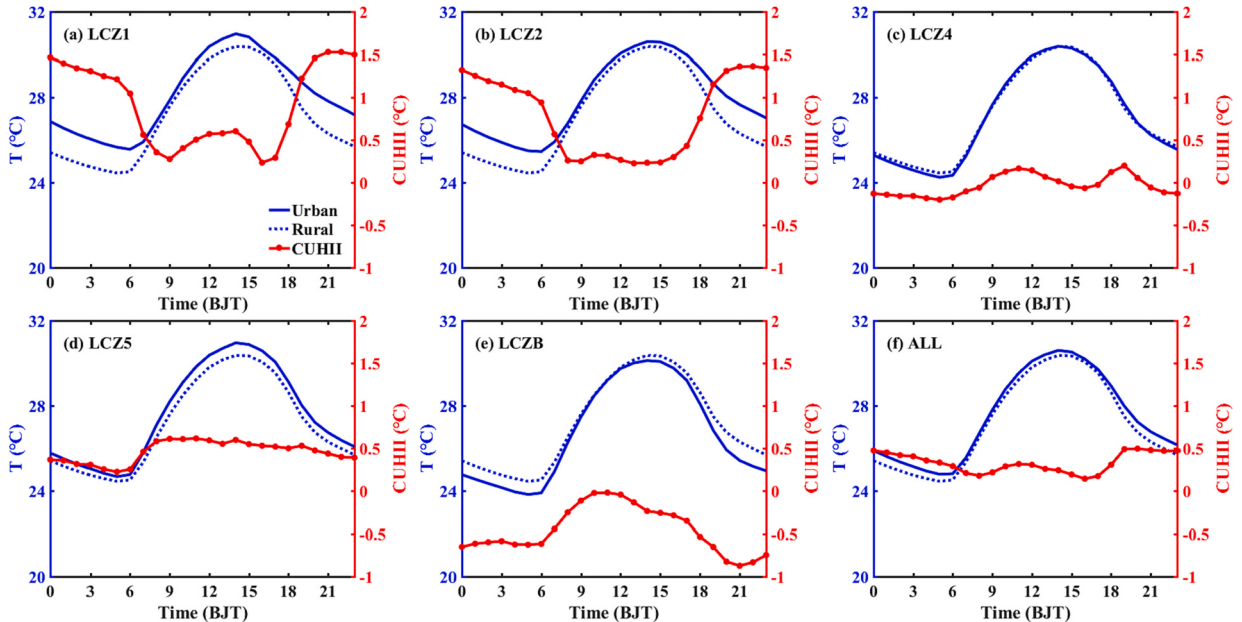


Fig. 4. Diurnal variation characteristics of urban and rural air temperatures and CUHII in different LCZ groups in Nanjing (2015–2020).

parkland and wetland, with vegetation and water bodies, and the CUHII is significantly lower than that of the other stations (calculation of their CUHII gives negative values). These results verify previous conclusions that urban parks and wetlands with vegetation and water have played a certain role in alleviating urban heat (Zong et al., 2021; Zhou et al., 2019).

Fig. 4 shows the diurnal variation characteristics of the CUHII over different LCZ groups. For LCZ1 and LCZ2 (Fig. 4a and b), at the center of city, the CUHI is strong during nighttime, even exceeding 1 °C, and weak during daytime, exhibiting significant variation. For LCZ4 and LCZ5 (Fig. 4c and d), on the outskirts of the city, the CUHI only appears at the peak of human activities. For example, the CUHII of LCZ4 appears at 1200 LST and around 1900 LST during the peak commuting period. The CUHI of LCZ5 appears after sunrise and remains stable until the evening. The reason for this phenomenon is related to the specific location and meteorological conditions of the two LCZ5 stations, which is discussed in Section 4.3. The above results confirm the previous conclusion that anthropogenic heat emissions play a non-negligible role in CUHIs (Li and Zhao, 2012; Oke et al., 2017). Similarly, LCZB (Fig. 4e), as mentioned previously, has a significant cold island effect, due to its proximity to a park water body, which has a positive effect on the mitigation of urban heat.

In summary, the diurnal variation of the summer CUHI in Nanjing is significant on the spatiotemporal scale, and different LCZ groups show different effects on CUHII. In general, anthropogenic heat emissions and urban parks/wetlands with vegetation and water bodies play an important role in urban heat.

3.2. Interannual variation

Fig. 5 shows the interannual variation characteristics of CUHII in summer 2015–2020. Obvious interannual variation characteristics can be seen: in 2015–2019, Nanjing's CUHII roughly shows an increasing trend year by year; however, in 2020, the CUHII decreases significantly. In addition to the increase of anthropogenic heat caused by increased population (Fig. 6 (b)), the improvement of air pollution also has a positive contribution in the enhancement of CUHII during 2015–2019. Previous studies have shown that under higher aerosol loadings context, the aerosol radiative effect exceeds the aerosol dynamical effect in summer, and surface temperature cooling is stronger in urban areas than in rural areas, offsetting urban heating and thus weakening CUHII (Han et al.,

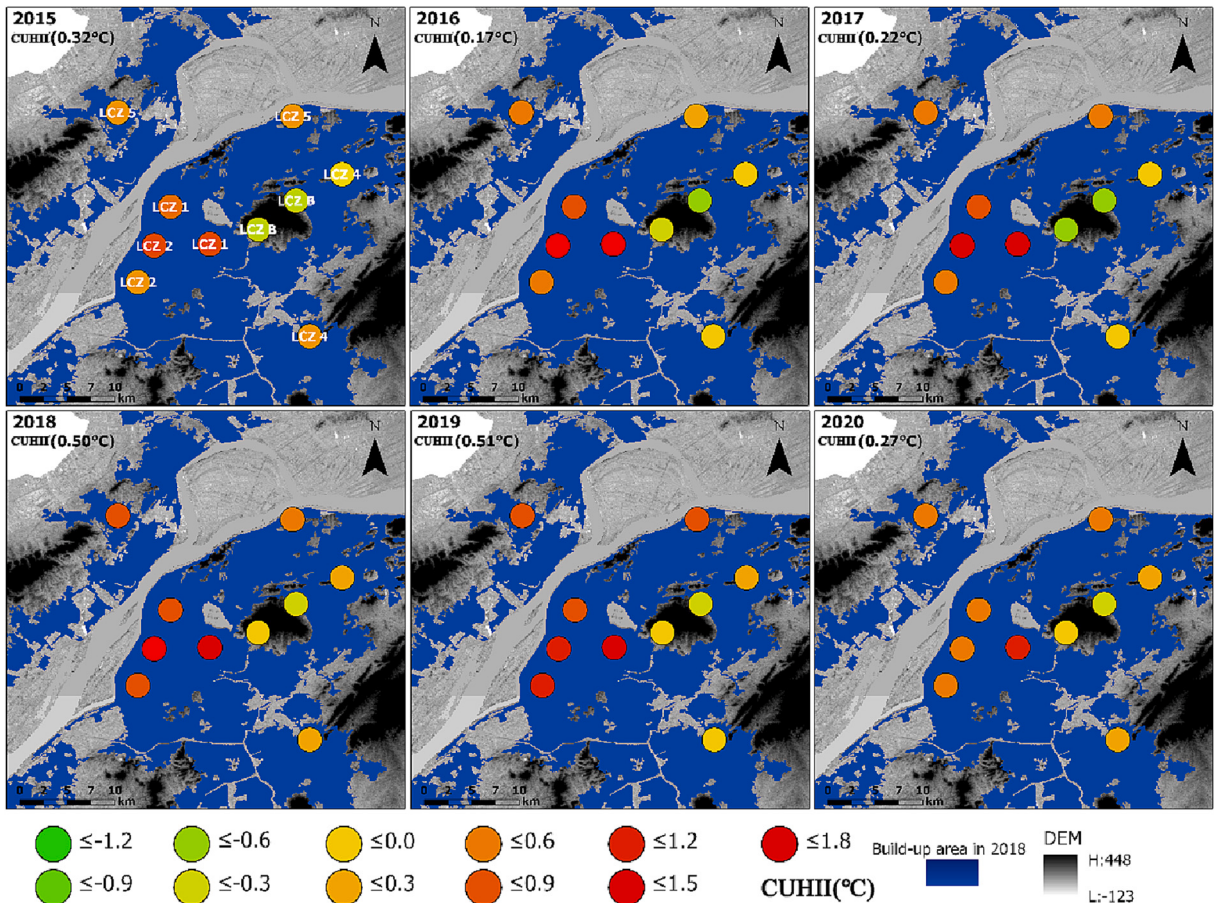


Fig. 5. Interannual variation characteristics of the CUHII in Nanjing. The mean UHII of 10 stations is shown in the top-left corner. The blue shading areas indicates the density of the built-up areas of Nanjing, and the gray-black shadings indicate altitudes. (For interpretation of the references to colour in this figure legend, the reader is referred to the web version of this article.)

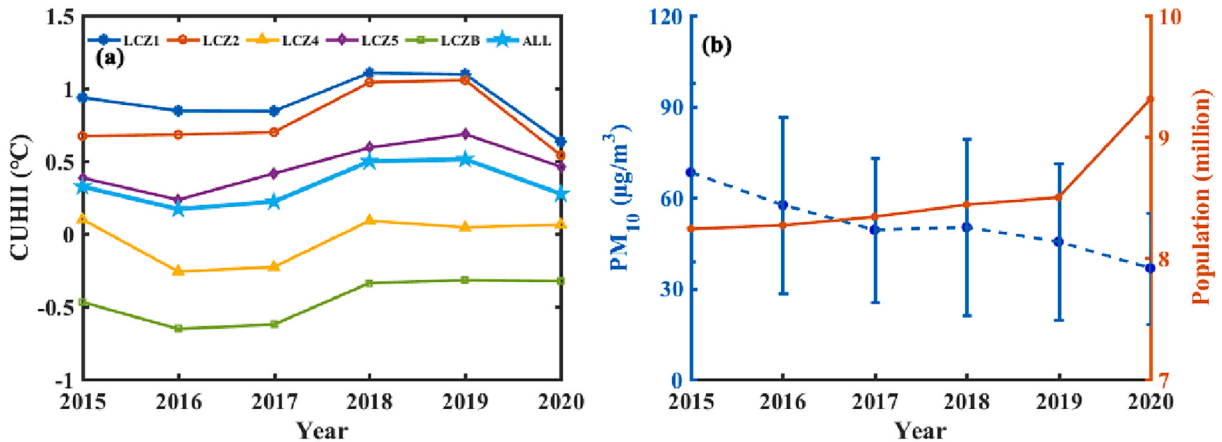


Fig. 6. interannual variation of (a) CUHII (b) AQI and population in Nanjing in summer (June–August) during 2015–2020.

2020; Yang et al., 2021), and vice versa. The summertime aerosol (particular matter) concentrations were decreasing over Nanjing during 2015–2019 (Fig. 6 (b)), which is favorable to enhance CUHII during the daytime (Wu et al., 2017; Zheng et al., 2018). Differently, in 2020, population/aerosol concentrations continued to increase/decrease, while CUHII decreased. According to previous studies (He et al., 2020; Teufel et al., 2021; Liu et al., 2022a), the actual decrease is due to a reduction in traffic heat emissions caused during the COVID-19 epidemic, resulting in weakened CUHII in 2020. In general, the interannual variability of CUHII was mainly dominated by anthropogenic heat emissions and air pollutions. Note that the impacts of interannual variability of synoptic weather pattern should not be ignored (Yang et al., 2022), which will be checked in our future work.

Fig. 6 (a) shows the interannual variation of CUHII averaged by the same LCZ group. In addition, to explore the cause of interannual variation of CUHII, we have supplied the interannual variations of population and particular matter concentrations (Fig. 6 (b)). Overall, the interannual variability of CUHII is similar for either LCZ. Downtown LCZ1 and LCZ2 with intensive human activity had CUHII exceeding 0.5 °C from 2015 to 2020. And during the pandemic, the interannual variation shifted from increasing to decreasing with a maximum variation of >0.5 °C. Compared to LCZ1 and LCZ2, LCZ4 and LCZB, located in less populated areas, did not show a significant decrease in CUHII during the pandemic, which again confirms that the influence of anthropogenic heat on CUHII is not negligible.

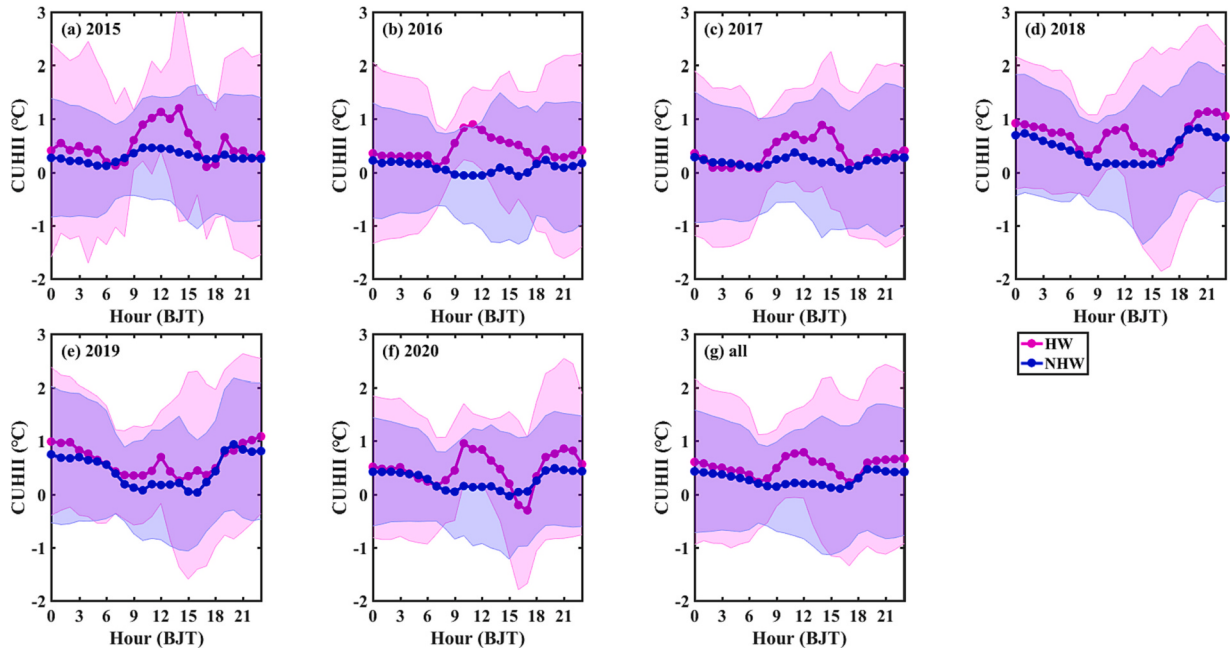


Fig. 7. Diurnal variation of CUHII in Nanjing during summer HW and NHW periods in 2015–2020. The HW (NHW) periods are shown in red (blue); the lines indicate the mean CUHII for all urban stations; and the shaded area indicates the standard deviation of the mean CUHII. (For interpretation of the references to colour in this figure legend, the reader is referred to the web version of this article.)

3.3. Synergy of CUHII–HW interaction

3.3.1. Differences in CUHII during the HW and NHW periods

In 2015–2020, the summer CUHII in Nanjing remains high at night and early morning, being weak in the daytime and showing a sub-peak at noon. Fig. 7 shows a “bimodal” daily variation, which is similar to the results of a previous study (Huang et al., 2008). During the HW period, the 6-yr mean CUHII for all urban stations ranges between 0.4 °C and 1 °C, and the mean CUHII during the NHW period ranges between 0.2 °C and 0.6 °C. The CUHII is significantly higher in the HW period than in the NHW period, indicating a clear synergy between HWs and CUHIs, which is also a positive feedback to HW intensity. This synergistic effect of CUHI–HW interaction is attributed to differential responses of the urban and rural surface energy balance to HWs and the mechanisms will be discussed in the Section 4.1.

3.3.2. Influences of LCZs on HWs and CUHIs

Fig. 8 shows the differences of CUHII in various LCZ groups at daytime and nighttime between HW and NHW periods. During the daytime (0600–1800 LST), the synergy of HW–CUHI interaction is significant for all LCZ groups, that is, the HW significantly enhances CUHII. The CUHII in both HW and NHW phases can be found as followings: LCZ1 > LCZ2 > LCZ4 > LCZB, while LCZ5 exhibits higher CUHII, which will be discussed in Section 4. During the nighttime, there are more significant synergistic effects of HW–CUHI interactions in LCZ groups in the city center, such as LCZ1 and LCZ2, where CUHII is significantly enhanced during the HW period relative to LCZ groups far from the city center, such as LCZ4, and LCZB. This is because that LCZ1 and LCZ2 are located in the city center, where are mainly dominated by concrete and steel, which store heat in the urban canopy layer at daytime, and then the heat is released at nighttime to warm the city (Li et al., 2015; Wang et al., 2020b). While for LCZ4 and LCZB being in a peri-urban area, strong daytime radiation causes continuous transpiration of plants or water body, resulting in an increase in latent heat flux and a decrease in CUHII during the HW period (Krich et al., 2022; Xian-Xiang and Xuan, 2021). In summary, synergistic effects of HW–CUHI interactions varied with different LCZ groups.

Furthermore, ANOVA testing for differences in UHII under the five LCZs shows $F(5509) = 1254.3$, $p < 0.001$, indicating that the CUHII under the five LCZs differs greatly.

3.4. Influences of WS on HWs and CUHIs

3.4.1. Variations in HW days under various WS conditions

To explore the modulation of CUHII, HWs, and their interactions by WS, the WS data from the national station (58238) was classified into three categories by a k-means clustering algorithm: low WS (0–2.2 m/s), medium WS (2.2–3.5 m/s), and high WS (> 3.5 m/s) (Fig. 9). The number of days of HW occurrence at low, medium, and high WS were separately counted, revealing a roughly

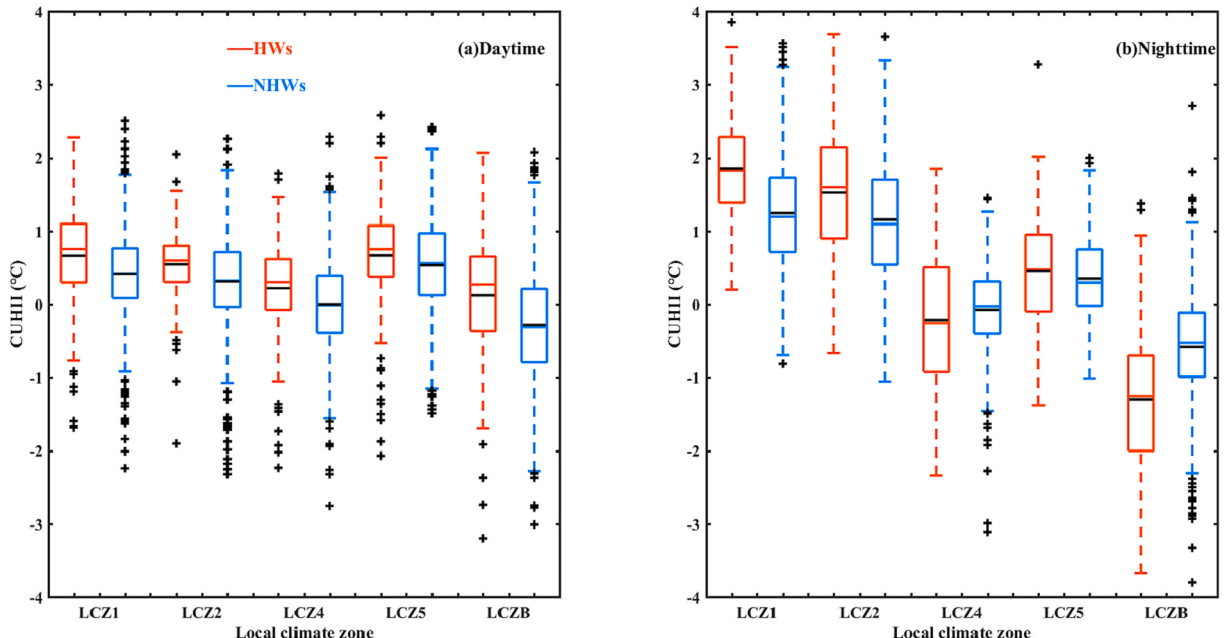


Fig. 8. Differences in CUHII during the HW and NHW periods in different LCZ groups, during the (a) daytime and (b) nighttime, respectively. The central box of the box plot indicates the values from the bottom to the top quartile (25th to 75th percentile); the dotted line extends from the maximum to the minimum; the solid line in the middle represents the median; the solid black line in the middle represents the mean; and the black plus signs represent outliers.

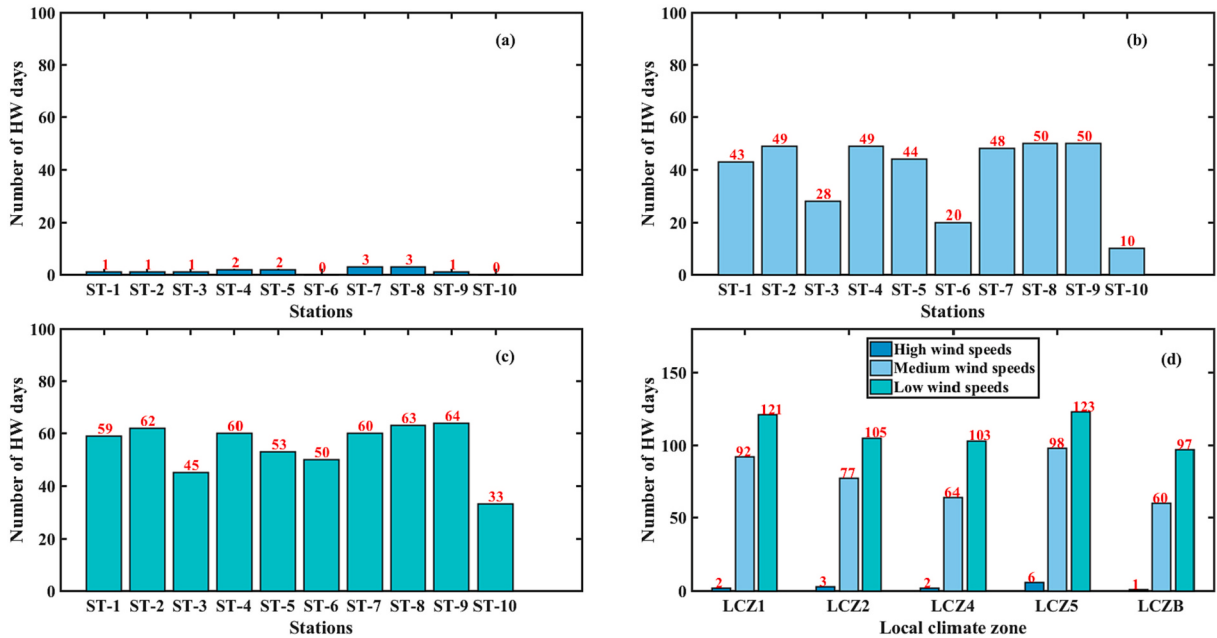


Fig. 9. Number of HW days under (a) high WS, (b) medium WS, and (c) low WS, at each urban station during 2015–2020. (d) Number of HW days occurrence under different LCZ groups, with dark to light colors representing high, medium, and low WS, respectively, and the red numbers representing the number of days. (For interpretation of the references to colour in this figure legend, the reader is referred to the web version of this article.)

negative association of HW days with WS. At low WS, most sites have >50 days of HW occurrence, while at medium WS the number of days of HW occurrence is significantly less than the number of days of HW occurrence at low WS. At high WS, there are no stations with >10 days of HW occurrence.

In addition, the number of HW days at some stations on the outskirts of the city even exceed those of the downtown stations at medium and high WS. The number at stations on the outskirts of the city increases with increasing WS, and, even if not meeting the requirements of an HW, the mean air temperature increases according to our statistics (Table 2). This is the result of horizontal heat advection by wind within the city. In summary, the highest frequency of HW days is seen at low WS, and the lowest frequency at high WS. However, due to horizontal heat advection by wind, the frequency of HW days increases relatively at stations on the outskirts of the city under medium and high WS.

3.4.2. Variations in CUHII under different WS conditions

Fig. 10 shows the CUHII of each urban station under high, medium, and low WS. Corresponding to the HW above, ST-1 and ST-2 maintain a high level of CUHII at low and medium WS because they are located in the city center, where the WS is more obstructed by buildings and heat is not easily advected (Chen et al., 2020; Li et al., 2011). The CUHII at all other stations basically increases with increasing WS. The sensitivity of CUHII to WS is highly dependent on the energy balance (Li et al., 2016). The occurrence of this difference we illustrate in the discussion. In addition, the above results are verified by ANOVA testing, in which the mean UHII differences among the three WS groups are statistically significant [$F(11029) = 107.15, p < 0.001$], indicating significant differences in UHII under different WSs.

Table 2

The mean air temperature under high, medium and low WS at each LCZ during 2015–2020.

LCZ	Low	Medium	High
LCZ1	28.14	27.99	27.71
LCZ2	27.91	27.98	27.72
LCZ4	27.11	27.14	27.08
LCZ5	27.59	27.63	27.63
LCZB	26.68	26.70	26.82

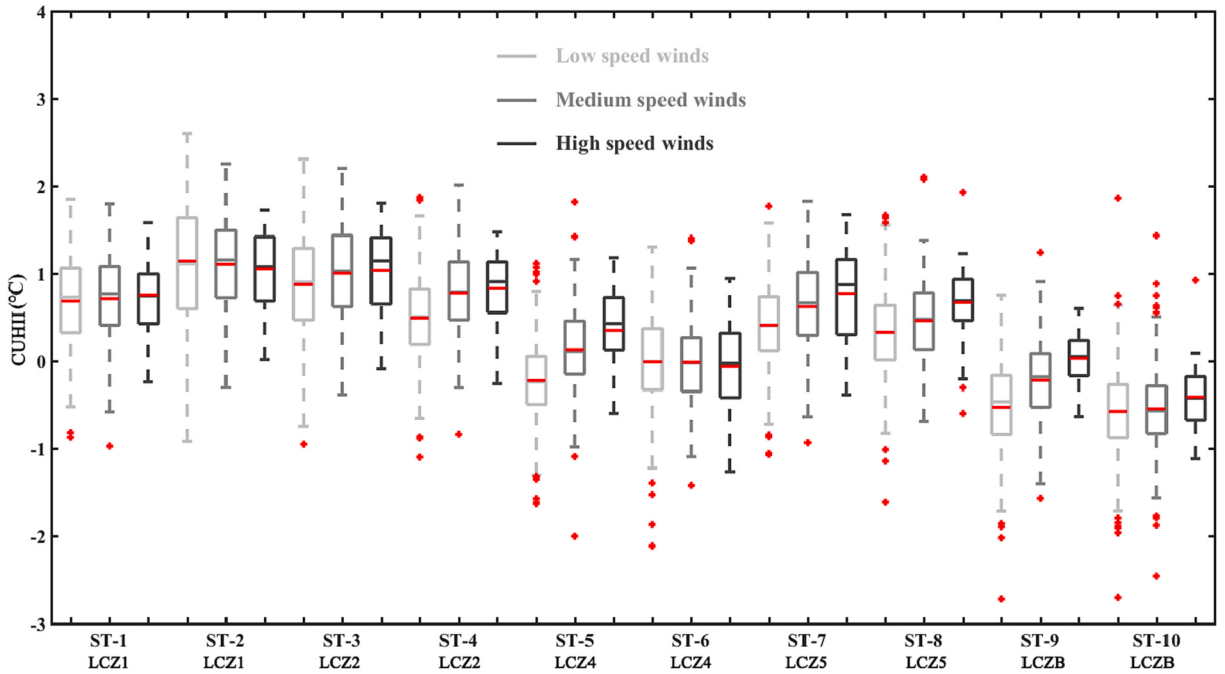


Fig. 10. The CUHII under high, medium and low WS (dark to light colors) at each urban station during 2015–2020. The central box of the box plot indicates the values from the bottom to the top quartile (25th to 75th percentile); the dotted line extends from the maximum to the minimum; the solid black line in the middle represents the median; the solid red line in the middle represents the mean; and the red plus signs represent outliers. (For interpretation of the references to colour in this figure legend, the reader is referred to the web version of this article.)

4. Discussion

4.1. Physical drivers of HW–NHW differences

In particular, during the HW period, CUHII exacerbates the risk of urban warming, increases heat stress-related diseases, and causes thermal discomfort, while increasing the need to use air conditioning (which significantly increases energy consumption) (Ngarambe et al., 2021). In Section 3.3, the diurnal variation in CUHII in the summers of 2015–2020 during HW and NHW periods in Nanjing was analyzed, and as expected, the CUHII in the HW periods is significantly stronger relative to the NHW periods, especially during daytime, which is a positive feedback to HW intensity. The physical cause of this phenomenon is the difference in the urban-rural

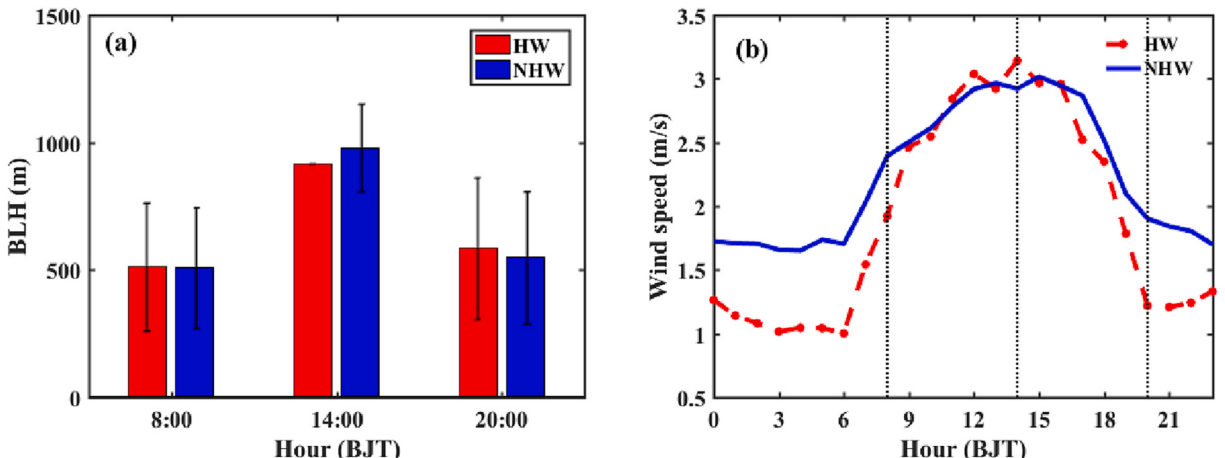


Fig. 11. The (a) BLH at 0800, 1400, and 2000 LST for the HW (red) and NHW (blue) periods, 2015–2018, with the solid black line representing the error range, and (b) daily variation in local WS for the HW (red) and NHW (blue) periods, 2015–2018, with the black dashed lines from left to right corresponding to the WS at 0800, 1400, and 2000 LST, respectively. (For interpretation of the references to colour in this figure legend, the reader is referred to the web version of this article.)

sensible heat flux and latent heat flux. Rural areas have greater latent heat flux during the daytime, and urban areas have greater sensible heat flux at night when the latent heat flux is close to zero in both urban and rural areas (Li et al., 2016; Zhao et al., 2018). During HWs, urban areas receive more short-wave and long-wave radiation than rural areas and store it in urban canopy layer, releasing more heat at night (Ding et al., 2010). This means that urban areas receive more heat than rural areas during HW periods compared to NHW periods, resulting in stronger CUHIs at night (Jiang et al., 2019). However, it is noteworthy that CUHII during the HW period shows a significant small peak at 0900–1500 LST compared to the NHW period (Fig. 7). This is different from the results of Ao et al. (2019), that is the enhanced daytime CUHII in Shanghai is due to the local onshore-sea wind circulation and the stable sea surface temperature during the day. In contrast, Nanjing is located inland, known as a “furnace”, and has a significantly higher frequency of artificial cooling during periods of high urban temperatures due to the use of air conditioning in places such as residential areas, shopping centers, and schools, resulting in more anthropogenic heat entering the air, thus leading to higher CUHII during the daytime (Zhao et al., 2018; An et al., 2020; Xu et al., 2018).

4.2. Meteorological drivers of HW–NHW differences

According to the data of the national station (58238) for the period 2015–2018, the causes of the differences between HW and NHW periods in terms of meteorological conditions were further explored (Fig. 11). In the morning (0800 LST) and evening (2000 LST), lower WSs with low boundary layer height (BLH) weaken the urban near-surface heat exchange and enhance the accumulation of heat, leading to greater CUHII (Fig. 3 and Fig. 7). Around the middle of the day (1400 LST), due to the higher BLH (Fig. 11) and sufficient WS conditions in urban areas, the CUHII is smaller (Fig. 3 and Fig. 7) (Yang et al., 2022). Compared to the NHW period, the lower boundary layer of the HW period results in heat accumulation in the urban canopy, which, combined with the lower WS that is not conducive to the mixing of heat, often results in high temperatures (Barlow et al., 2015; Zong et al., 2021; Wang et al., 2021).

4.3. UHA drivers of CUHI–HW interactions

The UHA by local wind was found to be another important factor for CUHI, HWs, and their interactions, in addition to the sensible and latent heat fluxes and the BLH. Modeling and observational studies of urban heat tend to assume that horizontal dispersion is similar throughout the city, and thus UHA is often neglected (Khan et al., 2020; Brousse et al., 2022). High WS usually dissipates heat accumulated in dense urban areas and decreases the magnitude of CUHI (Zong et al., 2021; Ngarambe et al., 2021); however, when the UHA by wind from warm areas of the city center is considered, the CUHII will be uncertain for different LCZs (Brousse et al., 2022; Khan et al., 2020). The central area of Nanjing is densely concentrated with buildings, and heat is advected horizontally between different LCZs by the wind. The heat is transported from the downtown area to the outskirts of the city, so the CUHII of this LCZ increases with increasing WS. For example, the heat of LCZ1 and LCZ2 heats other LCZs via advection, and the CUHII at the receiving stations appears to increase with increasing WS (Fig. 10).

In the present study, we used the stability of local winds to examine UHA, and the urban surface transport index (USTI) was defined to quantify the stability of winds and their ability to transport horizontal heat in the city. The value of USTI reflects the consistency of winds between each station within the city, ranging from 0 to 1. The more inconsistent the observed winds, the smaller the USTI. As shown in Fig. 12, ignoring the effects of anthropogenic activities and other potential drivers, an organized wind field within the city is more conducive to CUHII than a chaotic wind field at constant WSs; and a medium to high WS is more conducive to CUHII in a stable wind field. The effect of local wind on CUHI–HW interaction can be determined by considering the prevailing wind direction, WS, and USTI. In summary, high CUHII and multiple HWs usually occur with large USTI and medium to high WS, and UHA should be considered as an important contributor. When USTI values are small and the WS is weak, local heat accumulation should be considered.

Fig. 13 shows the correspondence between CUHII and local WS and wind direction for the outer urban stations. UHA should be considered as a significant contributor. Stations under LCZ4, LCZ5, and LCZB show stronger CUHI with increasing WS in some specific directions. However, LCZ5 appears in special situations, not only with strong CUHI along the downtown direction, but also with obvious CUHI in other directions. The reason for this difference was investigated and found to be the presence of a large number of factories around the ST-7 site, which resulted in significantly more anthropogenic heat emissions compared to the other sites. Similarly, ST-8 is located at a traffic hub with many highway overpasses, and such levels of traffic cause huge heat emissions.

4.4. Urban-ventilation drivers of CUHI–HW interactions

To assess the ventilation capacity of different LCZs, the WS ratio (WSR) index was introduced [WSR = WS/WS_r (Liu et al., 2022b; Yang et al., 2013)]. The closer the value of WSR is to 0, the stronger the weakening of WS by urbanization. Fig. 14 shows the correlation between the daily average WSR and CUHII for the 10 urban stations. There is a significant negative correlation between the daily average WSR and CUHII ($R = -0.6974$), indicating that poor ventilation may make an important contribution to the high CUHII, with LCZ1 and LCZ2 being particularly significant. Heat accumulation in the city center due to poor ventilation dominates CUHI–HW interactions.

Pervailing meteorological conditions and different land uses are among the fundamental drivers of atmospheric radiative and turbulent exchange, and their physical causes of the contribution of urban heat can be explained (Ngarambe et al., 2021). We can better understand their roles in CUHII–HW interaction by the flow chart depicted in Fig. 15.

In addition, Table 3 shows a two-way ANOVA for the effect of local WS and LCZs on CUHII. It can be seen that there is a significant

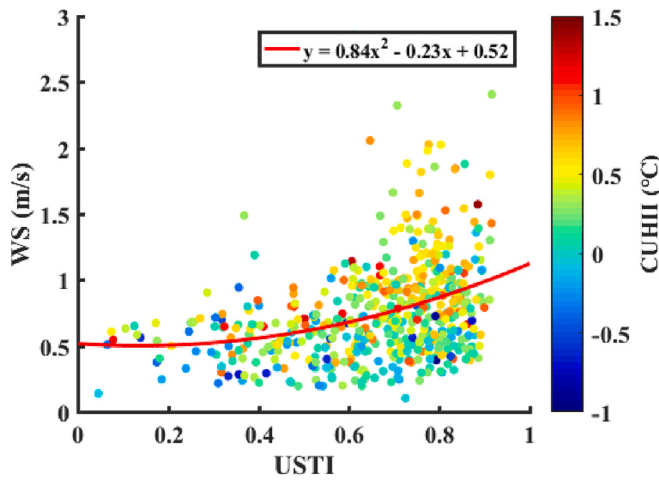


Fig. 12. USTI and daily mean CUHII during 2015–2020.

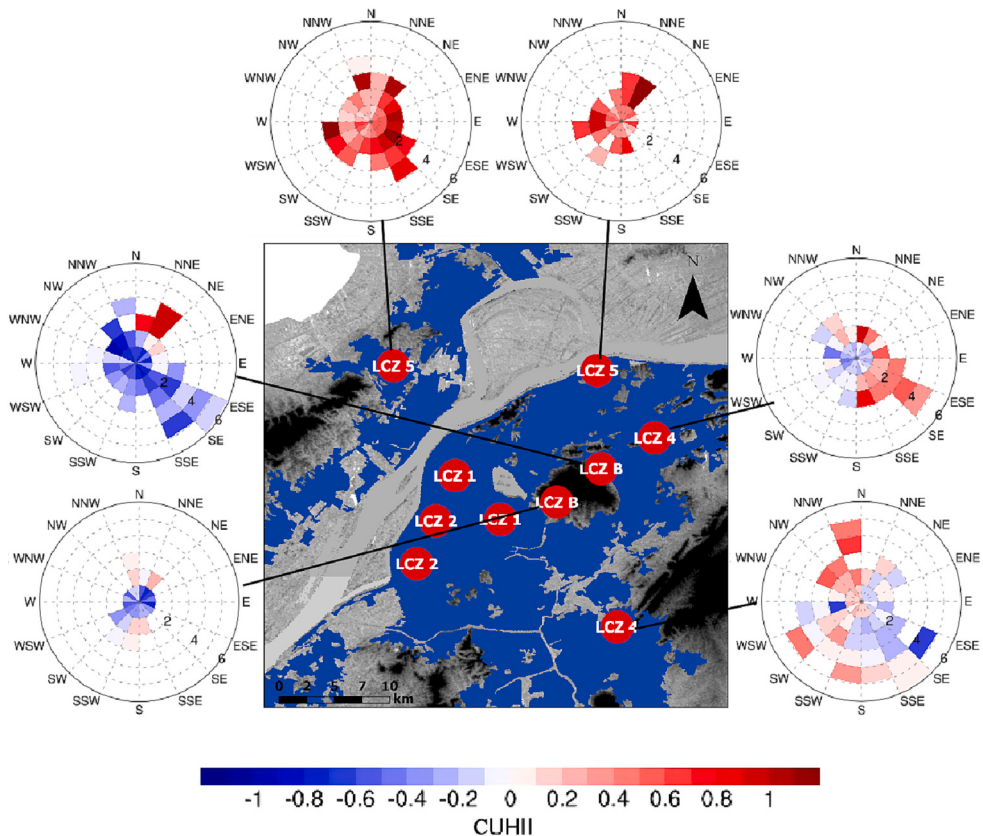


Fig. 13. Correspondence between CUHII and local WS and wind direction for the outer urban stations. The blue shading areas indicates the density of the built-up areas of Nanjing, and the gray-black shadings indicate altitudes. (For interpretation of the references to colour in this figure legend, the reader is referred to the web version of this article.)

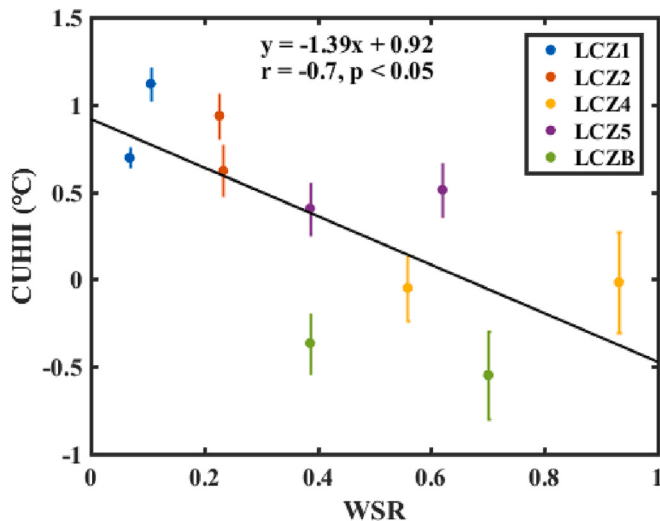


Fig. 14. Scatterplot of relationships between daily mean WSR and CUHII, in which the solid line indicates the standard deviation of the mean CUHII.

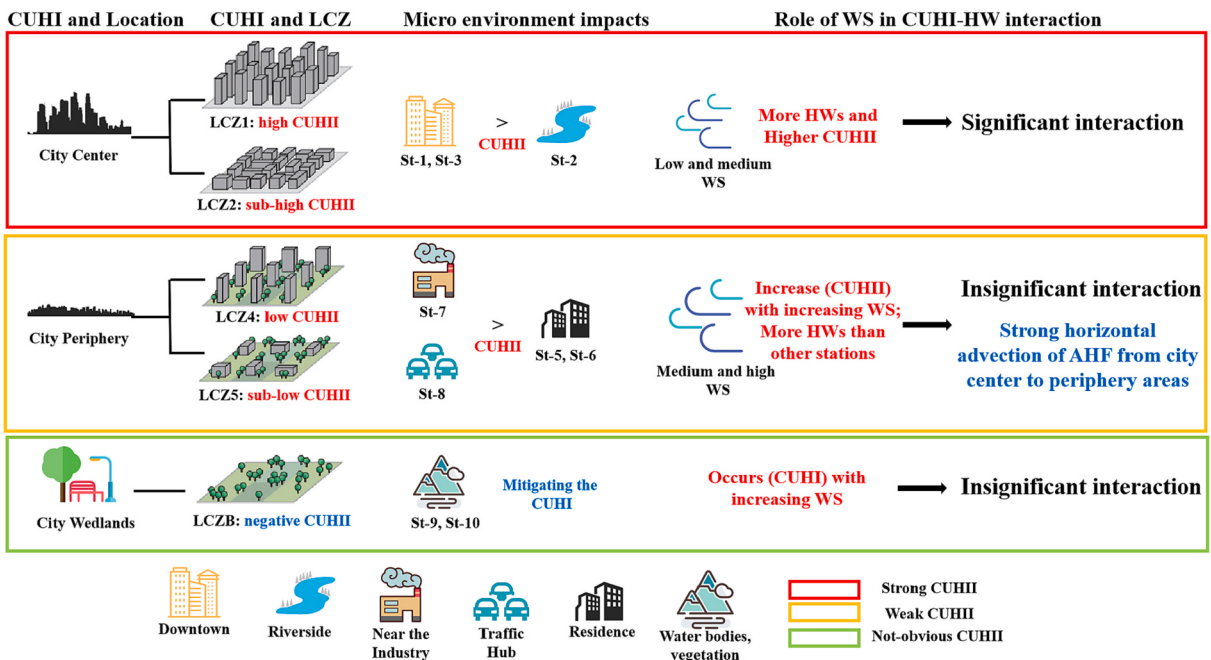


Fig. 15. Schematic diagram of the roles of LCZs and WS in CUHI-HW interaction.

Table 3
Two-way ANOVA between WS and LCZs to CUHII.

Source	Sum Sq	d.f	Mean Sq	F	Prob > F
WS	1082.7	2	541.34	512.42	0
LCZ	12,312.7	4	3078.18	2913.71	0
WS*LCZ	1248.5	8	156.07	147.73	0
Error	137,981.4	130,609	1.06		
Total	176,471	130,623			

difference in mean CUHII under the interaction of WS and LCZs [$F(8) = 147.73, p < 0.001$]. This is strong evidence for the roles played by LCZs and local WS in CUHII, and that LCZs are more sensitive to the magnitude of CUHII.

5. Conclusion

Based on observations from automatic meteorological stations in Nanjing during the summers of 2015–2020, this paper explores the diurnal and interannual variability of Nanjing's CUHI and their interaction with HWs, as well as the potential drivers. The main conclusions can be summarized as follows:

There is significant diurnal variation in the CUHI in summertime in Nanjing, showing a peak mean CUHII of around 0.5 °C during 2000–2100 LST, and a minimum mean CUHII of around 0.15 °C during 1500–1600 LST. This diurnal pattern is significant on the spatiotemporal scale and different LCZ groups show different effects on the CUHII, urban parks and wetlands with vegetation and water bodies play an important role in mitigating urban heat. The CUHII is significantly stronger in the HW periods than in the non-heat-wave (NHWs) periods, especially in the daytime, which is a positive feedback to HW intensity. The interannual variability of CUHII was mainly dominated by anthropogenic heat emissions and air pollutions.

While the spatial patterns of mean CUHII and HWs were shaped by LCZs and urban ventilation. Over LCZs with high densities of buildings in the city center, the CUHII is higher and HWs are more frequent under medium-low WS than high WS, and heat accumulation due to poor urban ventilation is an important contributor. In contrast, over LCZs with an open distribution of buildings, such as on the outskirts of the urban, under high WS condition, CUHII becomes higher and HW events become more frequently relative to low WS, due to the UHA induced by wind.

Overall, our results have important implications for subtropical, riverine, inland cities. The prediction of CUHII and HWs, and the assessment of the impact of the frequent CUHII drivers, as well as the prevention of summer heat hazards caused by CUHII and HWs, are valuable. Our findings suggest that both urban ventilation variability (e.g., various wind vectors) and anthropogenic activities (e.g., anthropogenic heat fluxes and LCZs) play an important role in the formation and development of urban climate in the complex context of the coupling between the land, atmosphere, and anthroposphere.

Funding

This research was supported by the National Natural Science Foundation of China (grant no. 42075098).

CRediT authorship contribution statement

Weishou Tian: Methodology, Software, Validation, Formal analysis, Writing – original draft, Writing – review & editing, Visualization. **Yuanjian Yang:** Conceptualization, Methodology, Validation, Formal analysis, Writing – review & editing, Supervision, Funding acquisition. **Linlin Wang:** Conceptualization, Data curation, Formal analysis, Writing – review & editing. **Lian Zong:** Formal analysis, Writing – review & editing. **Yanhao Zhang:** Formal analysis, Writing – review & editing. **Duanyang Liu:** Data curation, Formal analysis, Writing – review & editing.

Declaration of Competing Interest

The authors declare no conflict of interest.

Data availability

Landsat 8 OLI datasets (<http://www.gscloud.cn/sources/index?pid=263&rootid=1&label=Landsat8&sort=priority&page=1> (access on 10 April 2021)) were used to retrieve IS area, LULC and NDVI. nighttime light satellite datasets (<http://ngdc.noaa.gov/eog/dmsp/downloadV4composites.html> (access on 10 April 2022)) were used to retrieve anthropogenic heat flux (AHF), surface meteorological observations were collected from the China Meteorological Data Service Center (<http://data.cma.cn/en> (access on 10 April 2022)), DEM were achieved from geospatial data cloud (<http://www.gscloud.cn/sources/index?pid=302> (access on 10 April 2022)))

References

- An, N., Dou, J., González-Cruz, J.E., Bornstein, R.D., Miao, S., Li, L., 2020. An observational case study of synergies between an intense heat wave and the urban heat island in Beijing. *J. Appl. Meteorol. Climatol.* 59 (4), 605–620. <https://doi.org/10.1175/JAMC-D-19-0125.1>.
- Ao, X., Wang, L., Zhi, X., Gu, W., Yang, H., Li, D., 2019. Observed synergies between urban heat islands and heat waves and their controlling factors in Shanghai, China. *J. Appl. Meteorol. Climatol.* 58 (9), 1955–1972. <https://doi.org/10.1175/JAMC-D-19-0073.1>.
- Arnfield, A.J., 2003. Two decades of urban climate research: a review of turbulence, exchanges of energy and water, and the urban heat island. *Int. J. Climatol.* 23 (1), 1–26. <https://doi.org/10.1002/joc.859>.
- Barlow, J.F., Halios, C.H., Lane, S.E., et al., 2015. Observations of urban boundary layer structure during a strong urban heat island event. *Environ. Fluid Mech.* 15, 373–398. <https://doi.org/10.1007/s10652-014-9335-6>.
- Basagana, X., Sartini, C., Barrera-Gómez, J., Dadavand, P., Cunillera, J., Ostro, B., Sunyer, J., Medina-Ramón, M., 2011. Heat waves and cause-specific mortality at all ages. *Epidemiology* 765–772. <https://doi.org/10.1097/EDE.0b013e31823031c5>.

- Berkovic, S., 2016. Synoptic classes as a predictor of hourly surface wind regimes: the case of the central and Southern Israeli Coastal Plains. *J. Appl. Meteorol. Climatol.* 55, 1533–1547. <https://doi.org/10.1175/JAMC-D-16-0093.1>.
- Black, E., Blackburn, M., Harrison, G., Hoskins, B., Methven, J., 2004. Factors contributing to the summer 2003 european heatwave. *Weather* 59, 217–223. <https://doi.org/10.1256/wea.74.04>.
- Brousse, O., Simpson, C., Walker, N., Fenner, D., Meier, F., Taylor, J., Heavenside, C., 2022. Evidence of horizontal urban heat advection in London using six years of data from a citizen weather station network. *Environ. Res. Lett.* 4, 044041 <https://doi.org/10.1088/1748-9326/ac5c0f>.
- Cedeño Laurent, J.G., Williams, A., Oulhote, Y., Zanobetti, A., Allen, J.G., Spengler, J.D., 2018. Reduced cognitive function during a heat wave among residents of non-air-conditioned buildings: an observational study of young adults in the summer of 2016. *PLoS Med.* 15 (7), e1002605 <https://doi.org/10.1371/journal.pmed.1002605>.
- Chen, K., Huang, L., Zhou, L., Ma, Z., Bi, J., Li, T., 2015. Spatial analysis of the effect of the 2010 heat wave on stroke mortality in Nanjing, China. *Sci. Rep.* 5 (1), 10816. <https://doi.org/10.1038/srep10816>.
- Chen, X., Jeong, S., Park, H., Kim, J., Park, C., 2020. Urbanization has stronger impacts than regional climate change on wind stilling: a lesson from South Korea. *Environ. Res. Lett.* 15, 054016 <https://doi.org/10.1088/1748-9326/ab7e51>.
- Chen, S., Yang, Y., Deng, F., Zhang, Y., Liu, D., Liu, C., Gao, Z., 2022. A high-resolution monitoring approach of canopy urban heat island using a random forest model and multi-platform observation. *Atmos. Meas. Tech.* 15, 735–756. <https://doi.org/10.5194/amt-15-735-2022>.
- Chew, L.W., Liu, X., Li, X.-X., Norford, L.K., 2021. Interaction between heat wave and urban heat island: a case study in a tropical coastal city, Singapore. *Atmos. Res.* 247, 105134 <https://doi.org/10.1016/j.atmosres.2020.105134>.
- Ding, T., Qian, W., Yan, Z., 2010. Changes in hot days and heat waves in China during 1961–2007. *Int. J. Climatol.* 30, 1452–1462. <https://doi.org/10.1002/joc.1989>.
- Doick, K.J., Peace, A., Hutchings, T.R., 2014. The role of one large greenspace in mitigating London's nocturnal urban heat island. *Sci. Total Environ.* 493, 662–671. <https://doi.org/10.1016/j.scitotenv.2014.06.048>.
- Founda, D., Santamouris, M., 2017. Synergies between urban heat island and heat waves in Athens (Greece), during an extremely hot summer (2012). *Sci. Rep.* 7 (1), 10973. <https://doi.org/10.1038/s41598-017-11407-6>.
- Francisco, E., Tol, R., Botzen, W., Jeffrey, S., 2017. Global economic impacts of climate variability and change during the 20th century. *PLoS One* 12 (2), e0172201. <https://doi.org/10.1371/journal.pone.0172201>.
- Gao, Z., Hou, Y., Chen, W., 2019. Enhanced sensitivity of the urban heat island effect to summer temperatures induced by urban expansion. *Environ. Res. Lett.* 9 <https://doi.org/10.1088/1748-9326/ab2740>.
- Guo, A., Yang, J., Sun, W., Xiao, X., Xia, Cecilia, J., Jin, C., Li, X., 2020. Impact of urban morphology and landscape characteristics on spatiotemporal heterogeneity of land surface temperature. *Sustain. Cities Soc.* 63, 102443 <https://doi.org/10.1016/j.scs.2020.102443>.
- Guo, M., Zhang, M., Wang, H., Wang, L., Li, Y., 2021. Dual effects of synoptic weather patterns and urbanization on summer diurnal temperature range in an urban agglomeration of East China. *Front. Environ. Sci.* 9, 672295 <https://doi.org/10.3389/fenvs.2021.672295>.
- Habeeb, D., Vargo, J., Stone, B., 2015. Rising heat wave trends in large us cities. *Nat. Hazards* 76 (3), 1651–1665. <https://doi.org/10.1007/s11069-014-1563-z>.
- Han, W., Li, Z., Wu, F., Zhang, Y., Guo, J., Su, T., Cribb, M., Fan, J., Chen, T., Wei, J., Lee, S.-S., 2020. The mechanisms and seasonal differences of the impact of aerosols on daytime surface urban heat island effect. *Atmos. Chem. Phys.* 20, 6479–6493. <https://doi.org/10.5194/acp-20-6479-2020>.
- He, B.-J., 2018. Potentials of meteorological characteristics and synoptic conditions to mitigate urban heat island effects. *Urban Clim.* 24, 26–33. <https://doi.org/10.1016/j.uclim.2018.01.004>.
- He, B.-J., Zhao, Z.-Q., Shen, L.-D., Wang, H.-B., Li, L.-G., 2019. An approach to examining performances of cool/hot sources in mitigating/enhancing land surface temperature under different temperature backgrounds based on Landsat 8 image. *Sustain. Cities Soc.* 44, 416–427. <https://doi.org/10.1016/j.jscs.2018.10.049>.
- He, G., Pan, Y., Tanaka, T., 2020. The short-term impacts of COVID-19 lockdown on urban air pollution in China. *Nat. Sustain.* 3, 1005–1011. <https://doi.org/10.1038/s41893-020-0581-y>.
- He, B.-J., Wang, J., Liu, H., Ulpiani, G., 2021. Localized synergies between heat waves and urban heat islands: implications on human thermal comfort and urban heat management. *Environ. Res.* 193 (11), 110584 <https://doi.org/10.1016/j.enres.2020.110584>.
- Hu, J., Yang, Y., Pan, X., Zhu, Q., Zhan, W., Wang, Y., et al., 2019. Analysis of the spatial and temporal variations of land surface temperature based on local climate zones: a case study in Nanjing, China. *IEEE J. Sel. Top. Appl. Earth Obs. Remote Sens.* PP(99), 1–11. <https://doi.org/10.1109/JSTARS.2019.2926502>.
- Huang, L., Li, J., Zhao, D., Zhu, J., 2008. A fieldwork study on the diurnal changes of urban microclimate in four types of ground cover and urban heat island of Nanjing, China. *Build. Environ.* 43 (1), 7–17. <https://doi.org/10.1016/j.buildenv.2006.11.025>.
- Huang, Q., Li, L., Lu, Y., Yang, Y., Li, M., 2020. The roles of meteorological parameters in shanghai's nocturnal urban heat island from 1979 to 2013. *Theor. Appl. Climatol.* 141 (1), 285–297. <https://doi.org/10.1007/s00704-020-03214-3>.
- Imran, H.M., Kala, J., Ng, A.W.M., Muthukumaran, S., 2019. Impacts of future urban expansion on urban heat island effects during heatwave events in the city of Melbourne in Southeast Australia. *Q. J. R. Meteorol. Soc.* 145, 2586–2602. <https://doi.org/10.1002/qj.3580>.
- Jiang, S., Lee, X., Wang, J., Wang, K., 2019. Amplified urban heat islands during heat wave periods. *J. Geophys. Res.-Atmos.* 124, 7797–7812. <https://doi.org/10.1029/2018JD030230>.
- Jingxin, Yao, Xuguang, Sun, Jianping, Tang, Yaqin, Ji, Yiming, Xu, Qun, Yang Xiu, 2020. Summer regional pentad heat wave in eastern China and their possible causes. *Front. Earth Sci.* <https://doi.org/10.3389/feart.2020.598027>.
- Kaloustian, N., Bechtel, B., 2016. Local climatic zoning and urban heat island in Beirut. *Proc. Eng.* 169, 216–223. <https://doi.org/10.1016/j.proeng.2016.10.026>.
- Khan, H.S., Paolini, R., Santamouris, M., Caccetta, P., 2020. Exploring the synergies between urban overheating and heatwaves (hws) in western Sydney. *Energies* 13, 470. <https://doi.org/10.3390/en13020470>.
- Krich, C., Mahecha, M.D., Migliavacca, M., Kauwe, M.D., Griebel, A., Runge, J., et al., 2022. Decoupling between ecosystem photosynthesis and transpiration: a last resort against overheating. *Environ. Res. Lett.* 17 (4) <https://doi.org/10.1088/1748-9326/ac583e>, 17 044013.
- Kumar, R., Mishra, V., 2019. Decline in surface urban heat island intensity in India during heatwaves. *Environ. Res. Commun.* <https://doi.org/10.1088/2515-7620/ab121d>.
- Li, D., Bou-Zeid, E., 2013. Synergistic interactions between urban heat islands and heat waves: the impact in cities is larger than the sum of its parts*. *J. Appl. Meteorol. Climatol.* 52 (9), 2051–2064. <https://doi.org/10.1175/JAMC-D-13-021>.
- Li, Y., Zhao, X., 2012. An empirical study of the impact of human activity on long-term temperature change in China: a perspective from energy consumption. *J. Geophys. Res.-Atmos.* 117, D17117. <https://doi.org/10.1029/2012JD018132>.
- Li, Z., Yan, Z.W., Tu, K., Liu, W.D., Wang, Y.C., 2011. Changes in wind speed and extremes in Beijing during 1960–2008 based on homogenized observations. *Adv. Atmos. Sci.* 28 (2), 408–420. <https://doi.org/10.1007/s00376-010-0018-z>.
- Li, D., Sun, T., Liu, M., Yang, L., Wang, L., Gao, Z., 2015. Contrasting responses of urban and rural surface energy budgets to heat waves explain synergies between urban heat islands and heat waves. *Environ. Res. Lett.* 10 (5), 054009 <https://doi.org/10.1088/1748-9326/10/5/054009>.
- Li, D., Sun, T., Liu, M., Wang, L., Gao, Z., 2016. Changes in wind speed under heat waves enhance urban heat islands in the Beijing metropolitan area. *J. Appl. Meteorol. Climatol.* 55 (11), 2369–2375. <https://doi.org/10.1175/JAMC-D-16-0102.1>.
- Liu, G., Zhang, L., He, B., et al., 2015. Temporal changes in extreme high temperature, heat waves and relevant disasters in Nanjing metropolitan region, China. *Nat. Hazards* 76, 1415–1430. <https://doi.org/10.1007/s11069-014-1556-y>.
- Liu, Z., Lai, J., Zhan, W., Bechtel, B., Voogt, J., Quan, J., et al., 2022a. Urban heat islands significantly reduced by COVID-19 lockdown. *Geophys. Res. Lett.* 49 <https://doi.org/10.1029/2021GL096842> e2021GL096842.
- Liu, Y., Xuan, C., Xu, Y., Fu, N., Xiong, F., Gan, L., 2022b. Local climate effects of urban wind corridors in Beijing. *Urban Clim.* 43, 101181. ISSN 2212-0955. <https://doi.org/10.1016/j.uclim.2022.101181>.
- Ma, A., Act, A., Pk, A., Gyo, B., Rfb, B., 2020. Analysis of the urban heat island under different synoptic patterns using local climate zones. *Build. Environ.* 185 <https://doi.org/10.1016/j.buildenv.2020.107268>.

- Manoli, G., Faticchi, S., Schlapfer, M., Yu, K., Crowther, T.W., Meili, N., Burlando, P., Katul, G.G., Bou-Zeid, E., 2019. Magnitude of urban heat islands largely explained by climate and population. *Nature* 573, 55–60. <https://doi.org/10.1038/s41586-019-1512-9>.
- Meehl, G.A., Tebaldi, C., 2004. More intense, more frequent and longer lasting heat waves in the 21st century. *Science* 305, 994–997. <https://doi.org/10.1126/science.1098704>.
- Ngarambe, J., Nganyiyimana, J., Kim, I., Santamouris, M., Young Yun, G., 2020. Synergies between urban heat island and heat waves in Seoul: the role of wind speed and land use characteristics. *PLoS One* 15. <https://doi.org/10.1371/journal.pone.0243571> (12 December).
- Ngarambe, J., Jin, W.O., Mi, A.S., Santamouris, M., Yun, G.Y., 2021. Influences of wind speed, sky conditions, land use and land cover characteristics on the magnitude of the urban heat island in Seoul: an exploratory analysis. *Sustain. Cities Soc.* 71 (1), 102953 <https://doi.org/10.1016/j.scs.2021.102953>.
- Oke, T.R., Rummans, K.E., 2000. Dynamics and controls of the near-surface heat island of Vancouver, British Columbia. *Phys. Geogr.* <https://doi.org/10.1080/02723646.2000.10642711>.
- Oke, T., Mills, G., Christen, A., Voogt, J., 2017. Urban climates. In: *Urban Climates*. Cambridge University Press, Cambridge, p. III. <https://doi.org/10.1017/9781139016476>.
- Perkins, S.E., Alexander, L.V., Nairn, J.R., 2012. Increasing frequency, intensity and duration of observed global heatwaves and warm spells. *Geophys. Res. Lett.* 39 (20), 20714. <https://doi.org/10.1029/2012GL053361>.
- Poumadère, M., Mays, C., Le Mer, S., Blong, R., 2005. The 2003 heat wave in France: dangerous climate change here and now. *Risk Anal.* 25 (6), 1483–1494. <https://doi.org/10.1111/j.1539-6924.2005.00694.x>.
- Pyrgou, A., Hadjinicolaou, P., Santamouris, M., 2020. Urban-rural moisture contrast: regulator of the urban heat island and heatwaves' synergy over a Mediterranean city. *Environ. Res.* 182 (Mar) <https://doi.org/10.1016/j.envres.2019.109102>, 109102.1–109102.12.
- Rizvi, S.H., Alam, K., Iqbal, M.J., 2019. Spatio-temporal variations in urban heat island and its interaction with heat wave. *J. Atmos. Sol. Terr. Phys.* 185, 50–57. <https://doi.org/10.1016/j.jastp.2019.02.001>.
- Santamouris, M., 2014. Cooling the cities—a review of reflective and green roof mitigation technologies to fight heat island and improve comfort in urban environments. *Sol. Energy* 103, 682–703. <https://doi.org/10.1016/j.solener.2012.07.003>.
- Santamouris, M., 2015. Analyzing the heat island magnitude and characteristics in one hundred Asian and Australian cities and regions. *Sci. Total Environ.* 512–513, 582–598. <https://doi.org/10.1016/j.scitotenv.2015.01.060>.
- Santamouris, M., 2020. Recent progress on urban overheating and heat island research. Integrated assessment of the energy, environmental, vulnerability and health impact. *Synergies with the global climate change*. *Energy Build.* 207, 109482 <https://doi.org/10.1016/j.enbuild.2019.109482>.
- Shafiei Shiva, J., Chandler, D.G., Kunkel, K.E., 2019. Localized changes in heat wave properties across the United States. *Earth's Future* 7 (3), 300–319. <https://doi.org/10.1029/2018EF001085>.
- Stewart, I.D., 2011. A systematic review and scientific critique of methodology in modern urban heat island literature. *Int. J. Climatol.* 31 (2), 200–217. <https://doi.org/10.1002/joc.2141>.
- Stewart, I.D., Oke, T.R., 2012. Local climate zones for urban temperature studies. *Bull. Am. Meteorol. Soc.* 93 (12), 1879–1900. <https://doi.org/10.1175/BAMS-D-11-00019.1>.
- Stewart, I., Oke, T.R., Krayenhoff, E.S., 2014. Evaluation of the 'local climate zone' scheme using temperature observations and model simulations. *Int. J. Climatol.* 34, 1062–1080. <https://doi.org/10.1002/joc.3746>.
- Tan, J., Zheng, Y., Tang, X., Guo, C., Li, L., Song, G., Zhen, X., Yuan, D., Kalkstein, A.J., Li, F., Chen, H., 2010. The urban heat island and its impact on heat waves and human health in Shanghai. *Int. J. Biometeorol.* 54, 75–84. <https://doi.org/10.1007/s00484-009-0256-x>.
- Teufel, B., Sushama, L., Poitras, V., Dukhan, T., Bitsuamlak, G., 2021. Impact of covid-19-related traffic slowdown on urban heat characteristics. *Atmosphere* 12 (2), 243. <https://doi.org/10.3390/atmos12020243>.
- Thompson, R., Hornigold, R., Page, L., Waite, T., 2018. Associations between high ambient temperatures and heat waves with mental health outcomes: a systematic review. *Public Health* 161, 171–191. <https://doi.org/10.1016/j.puhe.2018.06.008>.
- Tu, L., Qin, Z., Li, W., Geng, J., Yang, L., Zhao, S., et al., 2016. Surface urban heat island effect and its relationship with urban expansion in Nanjing, China. *J. Appl. Remote. Sens.* 10 (2), 026037 <https://doi.org/10.1117/1.JRS.10.026037>.
- United Nations, 2019. World Urbanization Prospects: The 2018 Revision. <https://doi.org/10.18356/b9e995fe-en>.
- Vicedo-Cabrera, A.M., Scovronick, N., Sera, F., Royé, D., Schneidereit, R., Tobias, A., Astrom, C., Guo, Y., Honda, Y., Hondula, D.M., Abrutsky, R., Tong, S., Coelho, M.D. S.Z.S., Saldiva, P.H.N., Lavigne, E., Correa, P.M., Ortega, N.V., Kan, H., Osorio, S., Gasparini, A., 2021. The burden of heat-related mortality attributable to recent human-induced climate change. *Nat. Clim. Chang.* 11 (6), 492–500. <https://doi.org/10.1038/s41558-021-01058-x>.
- Wang, Q., Hang, J., Fan, Y., Li, Y., 2020a. Urban plume characteristics under various wind speed, heat flux, and stratification conditions. *Atmos. Environ.* 239, 117774 <https://doi.org/10.1016/j.atmosenv.2020.117774>.
- Wang, L., Li, D., Zhang, N., Sun, J., Guo, W., 2020b. Surface urban heat and cool islands and their drivers: an observational study in Nanjing, China. *J. Appl. Meteorol. Climatol.* 59 (12), 1–44. <https://doi.org/10.1175/JAMC-D-20-0089.s1>.
- Wang, W., Chen, B., Xu, Y., Zhou, W., Wang, X., 2021. Urban heat islands in Hong Kong: bonding with atmospheric stability. *Atmos. Sci. Lett.* 22 (6), e1032 <https://doi.org/10.1002/asl.1032>.
- Wu, H., Wang, T., Riemer, N., Chen, P., Li, M., Li, S., 2017. Urban heat island impacted by fine particles in Nanjing, China. *Sci. Rep.* 7 (1), 11422. <https://doi.org/10.1038/s41598-017-11705-z>.
- Xian-Xiang, Li, Xuan, Liu, 2021. Effect of tree evapotranspiration and hydrological processes on urban microclimate in a tropical city: a WRF/SLUCM study. *Urban Clim.* 40, 101009 <https://doi.org/10.1016/j.ulclim.2021.101009>.
- Xu, W., Li, Q., Wang, X.L., Yang, S., Cao, L., Feng, Y., 2013. Homogenization of Chinese daily surface air temperatures and analysis of trends in the extreme temperature indices. *J. Geophys. Res. Atmos.* 118, 9708–9720. <https://doi.org/10.1002/jgrd.50791>.
- Xu, X., Chen, F., Shen, S., Miao, S., Barlage, M., Guo, W., Mahalov, A., 2018. Using WRF-urban to assess summertime air conditioning electric loads and their impacts on urban weather in Beijing. *J. Geophys. Res. Atmos.* 123, 2475–2490. <https://doi.org/10.1002/2017JD028168>.
- Xz, A., To, B., Chao, R.C., Meng, C.D., Yi, A., Hw, E., et al., 2020. Evaluation of urban heat islands using local climate zones and the influence of sea-land breeze. *Sustain. Cities Soc.* 55 <https://doi.org/10.1016/j.scs.2020.102060>.
- Yang, F., Qian, F., Lau, S.S.Y., 2013. Urban form and density as indicators for summertime outdoor ventilation potential: a case study on high-rise housing in Shanghai. *Build. Environ.* 70, 122–137. <https://doi.org/10.1016/j.buildenv.2013.08.019>.
- Yang, X., Yao, L., Jin, T., Peng, L.L.H., Jiang, Z., Hu, Z., et al., 2018. Assessing the thermal behavior of different local climate zones in the Nanjing metropolis, China. *Build. Environ.* 171–184 <https://doi.org/10.1016/j.buildenv.2018.04.009>.
- Yang, J., Jin, S., Xiao, X., Jin, C., Xia, J., Li, X., Wang, S., 2019. Local climate zone ventilation and urban land surface temperatures: towards a performance-based and wind-sensitive planning proposal in megacities. *Sustain. Cities Soc.* 47, 101487 <https://doi.org/10.1016/j.scs.2019.101487>.
- Yang, X., Chen, Y., Peng, L., Wang, Q., 2020. Quantitative methods for identifying meteorological conditions conducive to the development of urban heat islands - science direct. *Build. Environ.* 178 <https://doi.org/10.1016/j.buildenv.2020.106953>.
- Yang, G., Ren, G., Zhang, P., Xue, X., Tysa, S.K., Jia, W., et al., 2021. PM2.5 influence on urban heat island (UHI) effect in Beijing and the possible mechanisms. *J. Geophys. Res.-Atmos.* 126 <https://doi.org/10.1029/2021JD035227> e2021JD035227.
- Yang, Y., Guo, M., Ren, G., Liu, S., Zong, L., Zhang, Y., Zheng, Z., Miao, Y., Zhang, Y., 2022. Modulation of wintertime canopy urban heat island (CUHI) intensity in Beijing by synoptic weather pattern in planetary boundary layer. *J. Geophys. Res.-Atmos.* 127 <https://doi.org/10.1029/2021JD035988>.
- Yun, G.Y., Ngarambe, J., Duhirwe, P.N., Ulpiani, G., Paolini, R., Haddad, S., Vasilakopoulou, K., Santamouris, M., 2020. Predicting the magnitude and the characteristics of the urban heat island in coastal cities in the proximity of desert landforms. The case of Sydney. *Sci. Total Environ.* 709, 136068 <https://doi.org/10.1016/j.scitotenv.2019.136068>.
- Zhao, Lei, Oppenheimer, Michael, Zhu, Qing, Baldwin, Jane W., Ebi, Kristie L., Bou-Zeid, Elie, Guan, Kaiyu, Liu, Xu., 2018. Interactions between urban heat islands and heat waves. United States. <https://doi.org/10.1088/1748-9326/aa9f73>.

- Zheng, Z., Ren, G., Wang, H., Dou, J., Gao, Z., Duan, C., Li, Y., Ngarukiyimana, J., Zhao, C., Cao, C., Jiang, M., Yang, Y., 2018. Relationship between fine-particle pollution and the urban heat island in Beijing, China: observational evidence. *Bound.-Layer Meteorol.* 169, 93–113. <https://doi.org/10.1007/s10546-018-0362-6>.
- Zhou, W., Shen, X., Cao, F., Sun, Y., 2019. Effects of area and shape of greenspace on urban cooling in Nanjing, China. *J. Urban Plan. Dev.* 145 (4), 04019016. [https://doi.org/10.1061/\(ASCE\)UP.1943-5444.0000520](https://doi.org/10.1061/(ASCE)UP.1943-5444.0000520).
- Zong, L., Liu, S., Yang, Y., Ren, G., Li, Y., 2021. Synergistic influence of local climate zones and wind speeds on the urban heat island and heat waves in the megacity of Beijing, China. *Front. Earth Sci.* 9, 458. <https://doi.org/10.3389/feart.2021.673786>.